

## **Computational intelligence-based decision support system for glaucoma detection.**

**Karkuzhali S\*, Manimegalai D**

Department of Information Technology, National Engineering College, Kovilpatti, Tamil Nadu, India

### **Abstract**

Glaucoma is the second major cause of loss of vision in the world. Assessment of Optic Nerve Head (ONH) is very important for diagnosing glaucoma and for patient monitoring after diagnosis. Robust and effective Optic Disc (OD), Optic Cup (OC) detection is a necessary preprocessing step to calculate the Cup-To-Disc Ratio (CDR), Inferior Superior Nasal Temporal (ISNT) ratio and distance between optic disc center and optic nerve head (DOO). OD is detected using Region Matching (RM) followed by medial axis detection in fundus images. OD and OC segmentations are carried out by Improved Super Pixel Classification (ISPC), Adaptive Mathematical Morphology (AMM) and the effectiveness of the algorithm is compared with existing k-means and fuzzy C means (FCM) algorithm. Experiments show that OD detection accuracies of 100%, 98.88%, 98.88% and 100% are obtained for the DRIVE, DIARETDB0, DIARETDB1 and DRISHTI data sets, respectively. In this work, three statistically significant ( $p < 0.0001$ ) features are used for Naive Bayes (NB), k-Nearest Neighbor (k-NN), Support Vector Machine (SVM), Feed Forward Back Propagation Neural Networks (FFBPNN), Distributed Time Delay Neural Network (DTDNN), radial basis function exact fit (RBFEF) and Radial Basis Function Few Neurons (RBFNF) classifier to select the best classifier. It is demonstrated that an average classification accuracy of 100%, sensitivity of 100%, specificity of 100% and precision of 100% have been achieved using FFBPNN, DTDNN, RBFEF and RBFNF. With expert ophthalmologist's validation, Decision Support System (DSS) used to make glaucoma diagnosis faster during the screening of normal/ glaucoma retinal images.

**Keywords:** Glaucoma, Retina, Optic disc, Optic cup, Cup to disc ratio, ISNT ratio.

*Accepted on March 11, 2017*

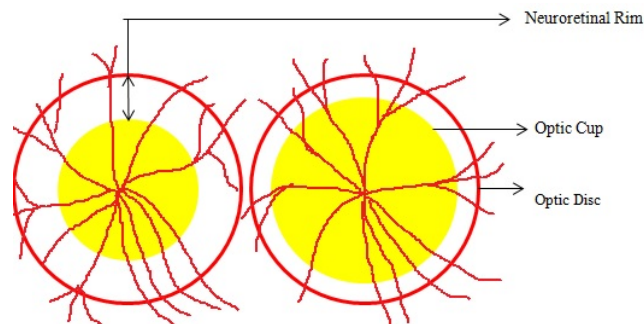
### **Introduction**

Glaucoma is a degenerative eye disease, in which the optic nerve is gradually damaged due to increased pressure causing loss of vision and eventually to a state of irreversible blindness [1]. According to World Health Organization, glaucoma is the second prime leading cause of blindness in the world [2]. The widespread model estimates that about 11.1 million people worldwide will suffer from glaucoma-induced irreversible blindness in 2020 [3]. Eye pressure occurs due to blockage in trabecular meshwork when aqueous humor flows in anterior chamber in the front part of our eye, plays a role in damaging the delegate nerve fibers of the optic nerve. Raised pressure inside the eye is called Intra Ocular Pressure (IOP) which has normal IOP of ~10 mmHg and glaucoma IOP > 20 mmHg, even patients with normal pressure can have glaucoma [4,5]. The design of Decision Support System (DSS) for glaucoma diagnosis depends on image cues and imaging modalities such as Optic Disc (OD) and Optic Cup (OC). OD is an oval brightest region in posterior chamber of the eye where ganglion nerve fibers assemble to form Optic Nerve Head (ONH). The center of OD has white cup-like area called OC [6]. The annular region between OD and OC is called as

Neuroretinal Rim (NR). The damage appears in optic nerve fibers leads to a change in the structural manifestation of the OD; the magnification of the OC (thinning of NR) is called cupping [7,8]. Figure 1 shows normal and abnormal retina. It may be mentioned here that glaucoma can be detected by measurement of IOP, visual field analysis and consideration of ONH. Assessment of damaged ONH is more effective and accurate to IOP measurement or visual field testing for glaucoma screening. Automatic ONH assessment plays a vital role in developing DSS for diagnosing glaucoma [9,10].

OD and OC detection is based on the detailed analysis of digital fundus images. In the diagnosis of glaucoma, considerable study has been carried out to find OD and OC in fundus images. There have been a number of reports available on color retinal images for detection of OD and OC [11-24]. The detection of glaucoma begins with preprocessing the retinal image, and localization of OD, which are followed by segmentation of OD and OC. The OD localization is carried out by Hough transformation [11] and Fourier transformation and p-tile for thresholding [12]. OD and OC segmentations by combination of Hough transform [12,13] and Active Contours Model (ACM) [12] have been reported. At the same time OD

and OC boundary detection by active snake model and active shape model [13] is also carried out. OD localization is done by illumination modification and boundary segmentation by a Supervised Gradient Vector Flow snake (SGVF) model [14]. OD localization and segmentation using template matching and level set method [15] are also implemented.



**Figure 1.** Diagrammatic representation of normal and glaucoma-affected retina.

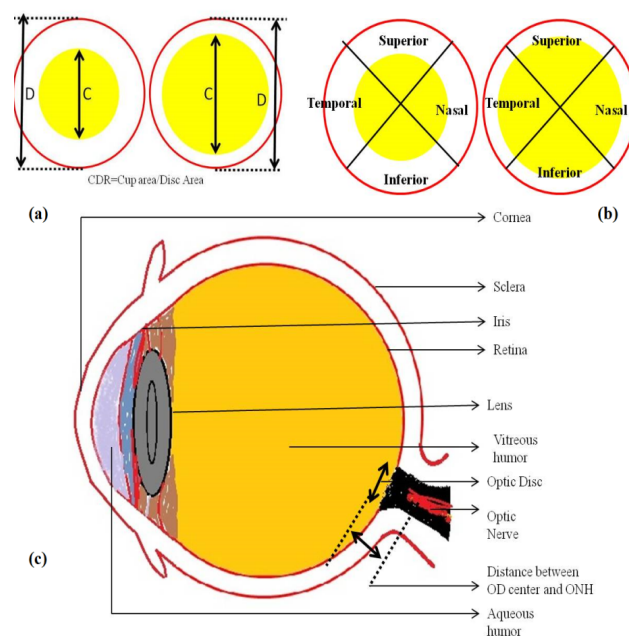
The localization of OD is carried out by selecting the significant scale-space blobs [16], and at the same time OD can be segmented by extracting the features such as compactness, entropy and blob brightness [16]. Comparison of OD segmentation algorithms such as ACM, fuzzy C means (FCM), and Artificial Neural Networks (ANN) has been reported [17]. A line operator has been used to capture circular brightness structure of OD [18]. However, a circular transformation is used to mark rounded contour and image dissimilarity across the OD [19]. Automated localization of the OD in color eye fundus images, has been extracted from the blood vessels with intensity data [20] and adaptive morphological two-stage approach [21]. The localization of OD has been performed using fast radial transform and vessel density estimation [22]. Interestingly, OC is segmented using multi-scale super pixel segmentation, and the boundary is detected using ellipse fitting algorithm [23]. Alternatively, OC can be segmented using motion boundary and its boundary by best circle fitting [24]. In the present investigation, a DSS system has been developed for detection of glaucoma using three clinical indicators such as Cup-to-Disc Ratio (CDR), Inferior Superior Nasal Temporal (ISNT) Ratio and distance between optic disc center and optic nerve head (DOO). CDR compares area of OC with area of OD. ISNT ratio is the relation between total area of vascular network in inferior and superior side of the OD to the total area of the vascular network in nasal and temporal areas [10]. Figure 2 shows the major structural indicators of glaucoma.

An attempt has been made to localize OD using Region Matching (RM). Subsequently, OD and OC segmentations have been carried out using Improved Super Pixel Classification (ISPC), Adaptive Mathematical Morphology (AMM) approach, k-means and FCM followed by feature vector formation and glaucoma classification by Naive Bayes (NB), k-NN (k-Nearest Neighbor), Support Vector Machine (SVM), Feed Forward Back Propagation Neural Networks (FFBPNN), Distributed Time Delay Neural Network

(DTDNN), Radial Basis Function Exact Fit (RBFEF) and Radial Basis Function Few Neurons (RBFNN).

## Materials and Methods

An attempt has been made here to develop a DSS to diagnose glaucoma. The assessment of ONH is carried by extracting image features for binary classification of healthy and glaucomatous subjects. During the assessment, the OD localization is an important preprocessing stage since it helps to localize and segment OD and OC to evaluate CDR, ISNT ratio and DOO. The localization of OD is carried out by preprocessing the input image and reference retinal image. The first step of preprocessing is to convert RGB to HSV image. Then, histogram equalization and histogram matching are applied in both the images to reduce uneven illuminations. The localization of OD is carried out using RM and k-NN search by Kd-trees; on the other hand the detection of OD centre is by medial axis (Scheme 1).

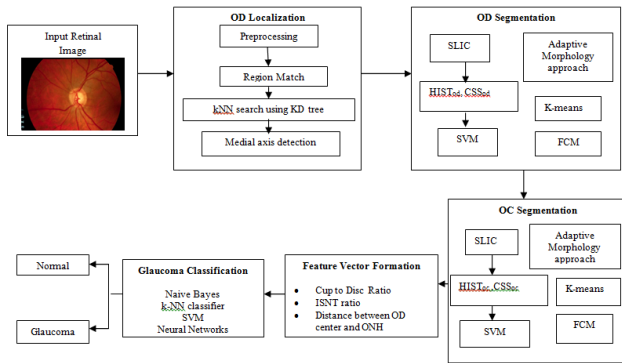


**Figure 2.** Diagrammatic representation of (a) CDR, (b) ISNT ratio for normal and abnormal retina (c) Distance between OD center and ONH.

In the segmentation of OD, Simple Linear Iterative Clustering (SLIC) is employed to aggregate pixels to super pixels. Further, the features like histograms and Center Surround Statistics (CSS) are extracted to classify each super pixel as OD or non-OD by SVM classifier. In order to compare the efficiency and accuracy of OD segmentation, AMM approach, k-means and FCM algorithms are used. Similarly, OC is also segmented by following the methodology adopted in segmentation of OD. Subsequently, the feature extraction is done by calculating CDR, ISNT ratio and DOO. Then, feature vector is formed using these three prime factors and given as an input for image classification and pattern recognition tasks (Scheme 1).

## Image acquisition

Drishti-GS data set (<http://cvit.iiit.ac.in/projects/mip/drishti-gs/mip-dataset2/Home.php>) consists of 101 images were collected from Aravind Eye Hospital, Madurai. The patients were between 40-80 years of age and OD centered images with dimensions of  $2896 \times 1944$  pixels. Expert annotated images were collected from ophthalmologist with clinical experience of 3, 5, 9 and 20 years [25].



**Scheme 1.** Flow diagram of the proposed approach.

## OD Localization using region match

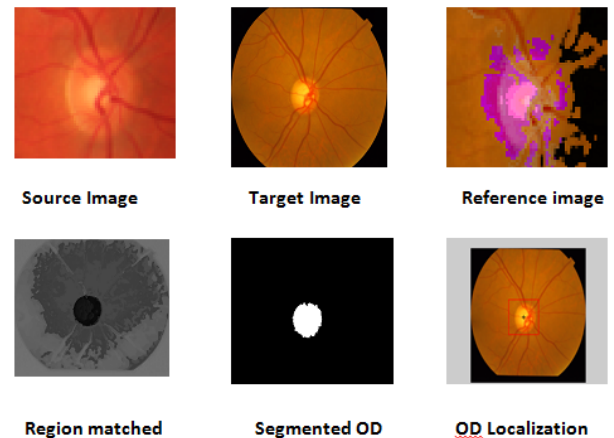
Before processing the retinal images for localization of OD, it is necessary to preprocess the retinal images to handle the illumination variations caused due to image acquisition under various conditions. Adaptive histogram equalization is used as preprocessing step to localize OD. Further, the RGB image is converted to grayscale. The histogram matching is performed between the cropped image (CI) and the Original Image (OI), and then the image is converted to HSV color space. In CI and OI, the correspondence map for every block is computed by block distance metric such as Euclidean distance. In RM, every block is approximated to a low dimensional feature, and these are used to find the nearest neighbor. The RM is computed by the following sequence: calculate the mean of R, G, B channels in the color fundus image, mean of X, Y gradients of the block, frequency components (first 2) of Walsh Hadamard Kernels and then finally the maximum value of the block.

The k-NN search has been performed effectively for low dimensional data using different categories of tree structures [8]. Construction of Kd-tree is done by the node points are iteratively partitioned into two sets at each node and by splitting along one dimension of the data until one of the termination criteria is met. Adaptive thresholding is used to segment OD. The OD is located by calculating the row center and column center by taking the average between the minimum number of rows/columns and the maximum number of rows/columns. The intersection point of row center and column center is marked as the OD center. Figure 3 shows the localization of OD using RM.

## OD segmentation and OC segmentation

**Improved super pixel classification:** The segmentation of OD is performed using ISPC. The SLIC algorithm is used to group

neighborhood pixels into super pixels in retinal fundus images. Histogram and CSS are used to classify each pixel as OD or non-OD in the segmentation of OD. It is worth mentioning that classification is performed using SVM. The output value is used as the assessment values for all pixels in the super pixel. Further, smoothed assessment values are used to obtain binary assessment values. Finally, +1, -1 and 0 are assigned to OD, non-OD and threshold respectively. Likewise, the resultant matrix with 1's and 0's is designated as OD and Non-OD (background) respectively [9].



**Figure 3.** Sample results of localization of OD using RM.

The following steps elaborately describe the ISPC for OD and OC segmentation.

Step 1: Compute SLIC by  $S = \sqrt{T/D}$  where T is the total number of super pixels, D is desired number of super pixels

Step 2: Compute histogram equalization for r, g, b from RGB color space and h, s from HSV color space  $HIST_j = (HIST_r, HIST_g, HIST_b, HIST_h, HIST_s)$ . The histogram computation counts number of pixels in 256 scales for R, G, B, H, and S to get 1280 dimensional features.

Step 3: Generate nine spatial scales dyadic Gaussian pyramids with a ratio from scale zero (1:1) to scale eight (1:256).

Step 4: Accomplish Low Pass Filter (LPF) version of Gaussian pyramid by convolution with separable Gaussian filter and decimation by factor 2.

Step 5: Compute CSS features as the mean and the variance of the maps within the super pixels.

Step 6: Expand CSS feature for  $SP_j$  to  $CSS_j = (CSS_j, CSS_{j1}, CSS_{j2}, CSS_{j3}, CSS_{j4})$ . It has a dimension of  $18 \times 2 \times 5 = 180$ .

Step 7: Combine the final feature (HISTOD, CSSOD) and (HISTOC, CSSOC).

Step 8: Assign output value for each super pixel as the assessment values for all pixels.

Step 9: Obtain the binary decisions for all pixels by smoothing decision values with a threshold.

Step 10: Assign +1 and -1 to OD and non-OD samples, and the threshold is the average of them, i.e. 0. 1 as OD and 0 as background.

**Adaptive mathematical morphology (AMM):** AMM is a non-linear image processing methodology and extracting ideas from set theory, topology and discrete mathematics. It is based on minimum (erosion) and maximum (dilation) operators whose aim is to extract the significant structures of an image with thresholding operation. The segmentation of OD and OC is carried out using combination of morphological operations and adaptive thresholding. Figure 4 shows results of ISPC and AMM. k-means and FCM algorithm performed using the steps carried out in our previous work [26].

The following steps describe clearly the sequence of morphological operations.

Step 1: Perform close and open operation in R and G components

Close-Fill the holes in lightest region both OD and OC region

Open-Remove any small light spots

Step 2: Separate disc and cup with standard deviation (SD) and Threshold value

R component-Threshold= $SD \times 3.2$

G component-Threshold= $SD \times 4.0$

Step 3: Calculate OD and OC area by adding the number of white pixels

Step 4: Detect OD center in cropped green channel image by thresholding

Step 5: Identify ONH coordinates by finding area of lightest intensity in bottom hat transformed OD cropped image

Step 6: Compute Euclidean distance between 2 points as distance between OD center and ONH

Step 7: Crop binary image of blood vessel to  $300 \times 300$

Step 8: Generate  $300 \times 300$  masks to cover 1 quadrant, rotated to 90 deg. each time to generate 4 masks

Step 9: Compute ISNT ratio by relation between area of vascular network enclosed by inferior and superior region to area of vascular network enclosed by nasal and temporal region of the cropped OD [10].

### Feature vector formation

The feature vector can be formed using three prime parameters as shown below [10]:

**CDR:** Cup-to-Disc Area Ratio (CAR)=OC area/OD area. (CDR>0.3 indicates the high risk of glaucoma)

**ISNT ratio:** ISNT ratio=Sum of vascular network area in inferior and superior regions/area of vascular network in nasal and temporal regions [10]. (Lower ISNT ratio increases the

risk of presence of glaucoma). Glaucoma damages superior and inferior first and then temporal and nasal optic nerve fibers, and it leads to decrease the area of vascular network in superior and inferior NR rim and change the order of ISNT (I S N T) relationship. Early diagnose of glaucoma was performed successfully by the detection of NR rim distances in inferior, superior, nasal and temporal directions to validate ISNT rule [27].

### Distance between ONH and OD center (DOO):

- The ONH coordinates are identified by locating the area of lightest intensity in OD cropped bottom hat transformed image.
- Similarly, the OD center is also detected by recognizing the area of pixels with lightest intensity.
- The Euclidean distance between OD center and ONH is computed to detect DOO. DOO is high for normal eye.

### Glaucoma classification

In the present work, seven classifiers, namely NB [3], k-NN, SVM [3], FFBPNN [10], DTDNN [28], RBFEF [28] and RBFFN have been employed to classify glaucoma. The retinal images are classified as normal or glaucoma using appropriate tools based on its features. The images marked as normal or abnormal with the aid of k-NN, SVM, NB, neural network tools available in MATLAB software. The glaucoma affected retinal images are classified using the statistically significant features such as CDR (<0.3, >0.3), ISNT rule (high/low) and DOO (high/low). By using k-NN classifier, a trained set, a sample set and a group are created. Based on the trained set, the samples are classified into normal and glaucoma cases [25]. In SVM classifier, v-SVM is used with penalization parameter  $v=0.5$  and cost parameter  $c=1$  [3]. Feed forward back propagation neural networks (FFBPNN), Distributed time-delay neural network (DTDNN), Radial basis function exact fit (RBFEF), Radial basis function few neurons RBFFN contains three layers, which are input, hidden and output layer. Three nodes for input layer, hidden neurons are set as 6, and output layer has 2 nodes which are normal and abnormal. RBFEF used for exact interpolation of data in multidimensional space and RBFFN used to achieve good accuracy with interpolation of few neurons [28]. There are three features are applied to the input layer for 26 images (13 is normal, 13 is abnormal) and the targets are set as normal and abnormal.

### Results and Discussion

In the present investigation, DRISHTI database with 101 images are used. Among the 101 images, 31 are normal and 70 are glaucoma cases. It is observed that ISPC algorithm is highly suitable for further processing. The statistical significance of features is analysed using student t-test. The outcome of the statistical test of the extracted features is shown in Table 1. It is clearly observed that, the features are statistically significant ( $p<0.0001$ ).

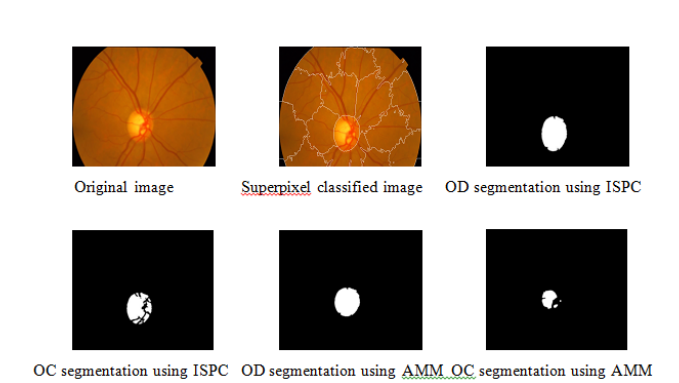


Figure 4. Sample results show segmentation of OD and OC using ISPC and AMM.

Training and testing set contains retinal images which are completely different and no overlapping found between them. To evaluate the performance of segmentation algorithms compared output of segmentation algorithm with expert annotated images. The performance evaluations for localization of OD are measured using Root Mean Square Error (RMSE), Structural Similarity Index Measure (SSIM) Equations 3 and 4 and for segmentation of OD are measured using sensitivity (SE), specificity (SPE), Accuracy (ACC), Precision (PRE), Error Rate (ER), f-score, classification accuracy (CA), Matthews Correlation Coefficient (MCC), Balanced Error Rate (BER), Misclassified Proportion (MP), Jaccard Coefficient (JC), Dice Coefficient (DC), False Positive Ratio (FPR), False Negative Ratio (FNR) Equations 1-9.

Table 1. Summary statistics of features used for normal and glaucoma groups.

Features	Normal (Mean ± SD)	Glaucoma (Mean ± SD)	P value
CDR	0.1942 0.0574	0.7539 0.1066	<0.0001
ISNT ratio	3.227 0.3617	1.120 0.4632	<0.0001
DOO	5553.00 511.53	1079 122.36	<0.0001

Table 2. Performance of the proposed localization algorithm.

Image ID	Original image	Segmented OD	Localized OD	SSIM	RMSE

$$RMSE = \frac{1}{N^2} \sum_{x=0}^{N-1} \sum_{y=0}^{N-1} (f(x,y) - \widehat{f}(x,y))^2 \rightarrow (1)$$

$$SSIM(x,y) = \frac{(2 \mu_x \mu_y + C_1)(2 \sigma_{xy} + C_2)}{(\mu_x^2 + \mu_y^2 + C_1)(\sigma_x^2 + \sigma_y^2 + C_2)} \rightarrow (2)$$

$$Sensitivity(SE) = \frac{TP}{TP + FN} \rightarrow (3)$$

$$Specificity(SPE) = \frac{TP}{TP + FN} \rightarrow (4)$$

$$Accuracy(ACC) = \frac{TP + TN}{TP + FN + TN + FP} \rightarrow (5)$$

$$Precision(PRE) = \frac{TP}{TP + FP} \rightarrow (6)$$

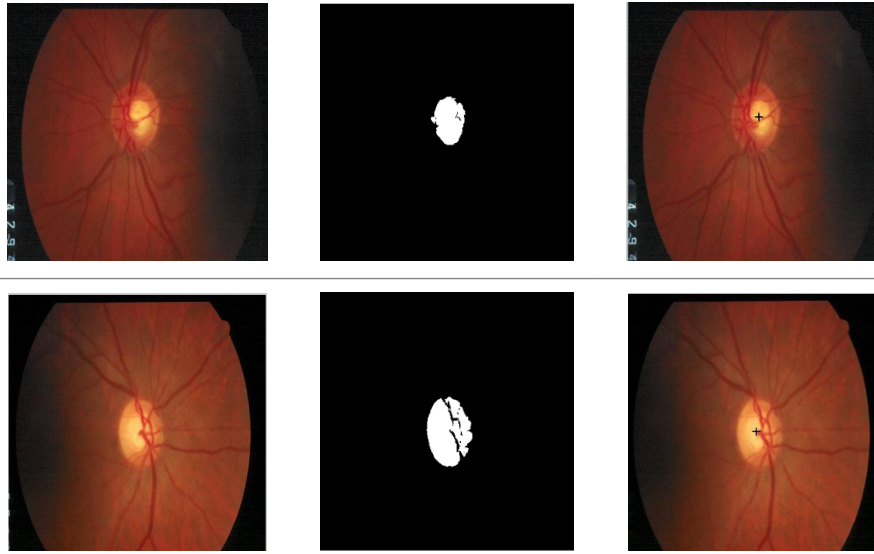
$$Error\ Rate = \frac{TP}{FP + FN + TP + TN} \rightarrow (7)$$

$$F - score = 2 \times \frac{(PRE \times SE)}{(PRE + SE)} \rightarrow (8)$$

Classification Accuracy (CA)=The probability (%) that the classifier has labeled an image pixel into the expert annotated class and its being correctly classified as such.

$$Mattews\ Correlation\ Coeffecient\ (MCC) = \frac{(TP \times TN - FP \times FN)}{\sqrt{((TP + FP) \times (TP + FN) \times (TN + FP) \times (TN + FN))}} \rightarrow (9)$$





$$\text{Balanced Error Rate (BER)} = 0.5 \times \left( \frac{FN}{TP + FN} + \frac{FP}{FP + TN} \right) \rightarrow (10)$$

$$\text{Misclassified proportion} = \frac{FP}{TP + FP + TN + FN} \rightarrow (11)$$

$$\text{Jaccard Coefficient } J(A, B) = \frac{|A \cap B|}{|A \cup B|} \rightarrow (12)$$

$$\text{Dice Coefficient } D(A, B) = \frac{2|A \cap B|}{|A| + |B|} \rightarrow (13)$$

$$\text{False Positive Ratio (FPR)} = \frac{|B| - |A \cap B|}{|A|} \rightarrow (14)$$

$$\text{False Negative Ratio (FNR)} = \frac{|A| - |A \cap B|}{|A|} \rightarrow (15)$$

Where,  $f(x, y)$ ,  $f'(x, y)$  Equation 6  $\mu_x$ ,  $\mu_y$ ,  $\sigma_x^2$ ,  $\sigma_y^2$ ,  $C_1$ ,  $C_2$ . Equation 7  $TP$ ,  $TN$ ,  $FP$ ,  $FN$  (Equations 12-16),  $A$  and  $B$  (Equations 10-15) are average differences between original image and segmented image, mean and covariance of segmented image and ground truth image, constants ( $C_1$  and  $C_2$ ), true positive, true negative, false positive, and false negative, segmented image and ground truth image respectively. If expert annotated image and segmented output are positive as positive and negative as negative, then it will be  $TP$  and  $TN$  respectively. If expert annotated image and segmented output are negative as positive and positive as negative, then it will be  $FP$  and  $FN$  respectively. With respect to this statistical treatment, SE is defined as the percentage of unhealthy image in expert annotation is classified as unhealthy in segmented output. SPE defined as the percentage of healthy image in expert annotation is classified as healthy in segmented output.

Tables 2 and 3 present the experimental results obtained by the OD localization and segmentation algorithm, which reveals that the algorithm yields hopeful results in terms of RMSE, SSIM, SE, SPE, ACC and PRE even though only low-quality images are used as test images. Average of the Equations 8-20 was calculated for all images in the data set to obtain the

overall performance measure (Table 3). Among the 101 images employed, 50 images are used for training and the remaining 51 images are used for testing. In the present work, out of the 51 images used for testing, 26 (13 are normal, 13 are glaucoma affected) images are used for evaluation. The FFBPNN, DTDNN, RBFEF and RBFFN classifier is used to classify 13 glaucoma-affected images as glaucoma and 13 normal images as normal. It is observed that the average classification rate is 100%, which is clinically significant.

Table 4 shows SE, SPE, ACC and PRE for the normal and glaucoma cases using seven classifiers. The FFBPNN, DTDNN, RBFEF and RBFFN classifier is able to detect abnormality with an SE of 100%, an SPE of 100% and PRE of 100%. Tables 5-7 show the comparison of OD localization and OD and OC segmentations algorithms for the present investigation with the reported results. Table 8 shows the tuning parameters for neural networks classifier. It is clearly seen from Table 5 that the RM algorithm for OD localization is highly suitable for DRIVE and DRISHTI database [29-36]. It may be mentioned here that many of the reports have used only CDR-ISNT ratio for the extraction of features [27,37-45], whereas in the present work, in addition to CDR-ISNT ratio, DOO is also computed. The segmentation of OD and OC requires computation time of 6.4s and 1.3s respectively. It is clearly seen from Table 6 that much less computation time is required in the present work than the results already reported by Cheng et al. [9]. It is also confirmed that much less overlapping error (2.12% for OD and 1.57% for OC) is observed than the report by Cheng et al. [9] (9.5% for OD and 24.1% for OC) and Yin et al. [41] (9.72% for OD and 32% for OC).

Extracting energy features obtained using 2D discrete wavelet transform subjects these signatures to various feature extraction and feature ranking methodologies. Five different classifiers such as LIBSVM, Sequential minimal optimization\_1 (SMO\_1), SMO\_2, Random Forest, NB are used for classification and they showed a ACC, PRE, SE, SPE

of {100% 100% 100% 100%}, {100% 100% 100% 100%}, {88.29% 81.82% 100% 100%} and {100% 100% 100% 100%} values respectively [3]. The localization of OD is performed using sliding window, a new histogram-based feature in machine learning framework. The support vector regression-based on RBF is used for feature ranking and non-maximal suppression for decision-making. The method is tested on ORIGA database, and achieved overlapping error, CDR error and Absolute area difference are 73.2%, 0.09 and 31.5 respectively [6]. Region growing with Active Contour Model (ACM) and vessel bend detection followed by 2D spline interpolation are used for segmentation of OD and boundary of OC. The method has been evaluated on 138 retinal images. They minimize estimation error for vertical CDR, CAR are 0.09/0.08 and 0.12/0.10 respectively [7]. The segmentation of OD and OC by SPC is followed by self-assessment reliability score and achieved average overlapping error 9.5% and 24.1% respectively. The method is evaluated with 650 images from two data sets and achieved area under curve 0.800 and 0.822 for them [9].

The mathematical morphology followed by thresholding is used for segmentation of OD, OC, blood vessels and ANN for classification of glaucomatous images. This method is able to distinguish normal and glaucoma classes with an SE of 100%

and SPE of 80% respectively [10]. Measurement of displacement of blood vessel within OD caused by the growth of OC is the prime factor for the assessment of glaucoma. Their system yielded an SE of 93.02%, SPE of 91.66%, AUC of 92.3% and accuracy of 92.34% [12]. Localization and segmentation of OD and OD boundary are carried out by illumination correction and SGVF snake model with overall performance of 95% and 91% respectively [14]. Segmentation and localization of OD are performed by region, local gradient information and template matching algorithm. This method yielded a success rate of 99%, and the total distance between result of boundary of segmented image and ground truth is 10% [15]. The decision tree, regression-based classifier and majority voting classifiers used features like compactness, entropy and blob brightness features from scale-space blob for identification of OD in retinal images. Their algorithm demonstrated an SE of 85.37% and PPV of 82.87% in the detection of OD [16]. Segmentation of OD is performed using three methods, namely ACM, FCM, ANN for calculating cup to disc ratio for glaucoma screening. Their system showed overlap measure {0.88, 0.87}, {0.88 0.89} and {0.86, 0.86} for all the images [17]. The designed line operator is used for detection of OD, which is characterized by circular brightness structure. This method showed accuracy with 97.4% [18].

**Table 3.** Performance of the proposed OD and OC segmentation algorithm.

Algorithm	OD Segmentation					OC Segmentation				
	ISPC	AMM	K algorithm	means	FCM	ISPC	AMM	K algorithm	means	FCM
Sensitivity (%)	97.17	94.44	96.23		97	94.56	88.61	88.91		93.41
Specificity (%)	95.87	84.74	91.27		85.43	93.65	82.59	82.44		83.26
Accuracy (%)	97.23	93.42	93.45		94.36	98.42	94.56	88.52		92.65
Precision (%)	99.999	99.991	99.99		99.994	99.996	99.996	99.993		99.993
Error rate	0.0212	0.0118	0.0116		0.0186	0.0157	0.0133	0.007		0.0063
F score (%)	99.989	99.994	99.994		99.99	99.9921	99.9933	99.9965		99.9969
Classification Accuracy (%)	99	99.34	97.84		99.16	98.072	98.388	98.353		98.307
Mathews Correlation Coefficient	0.8134	-0.0054	-0.5		0.15285	0.7483	0.1636	0.0004		0.0002
Balanced error rate	0.3637	0.5	0.5		0.3948	0.5	0.375	0.5		0.5
Misclassified Proportion	0.00003	0.0086	0.00908		0.00594	0.0003	0.00354	0.00703		0.00626
Jaccord coefficient	0.92304	0.8896	0.37382		0.8378	0.74896	0.6917	0.3149		0.37049
Dice coefficient	0.00402	0.00395	0.00327		0.0072	0.00393	0.0036	0.0032		0.00363
False positive rate	0.97915	0.92467	0.00341		0.00137	0.81433	0.73954	0.00032		0.0014
False negative rate	0.996	0.9961	0.9984		0.9964	0.99642	0.99684	0.984		0.9982

**Table 4.** Performance of classification algorithm.

Algorithm	TP	FN	TN	FP	SE	SPE	ACC	PRE
k-NN Classifier	13	0	12	1	100	92.3	96.15	92.85
Naive Bayes	11	0	13	2	100	86.66	92.3	100

SVM	12	0	13	1	100	92.85	96.15	100
FFBPNN	13	0	13	0	100	100	100	100
DTDNN	13	0	13	0	100	100	100	100
RBFEF	13	0	13	0	100	100	100	100

RBFFN	13	0	13	0	100	100	100	100
-------	----	---	----	---	-----	-----	-----	-----

**Table 5.** OD localization results for the proposed and literature reviewed methods.

Author name	Year	Ref	Algorithm	Database	Number images	of Computational time(s)	Accuracy (%)
Youssif et al.	2008	[29]	Vessel direction matched filter	STARE	81	-	98.77
				DRIVE	40		100
Niemeijer et al.	2009	[30]	Position regression based template matching	Local Database	1100	7.6	99.4
Aquino et al.	2010	[31]	New template-based method	Messidor	1200	1.67	99
Welfer et al.	2010	[32]	Adaptive morphological approach	DRIVE	40		100
				DIARETDB1	89	7.89	97.75
Mahfouz et al.	2010	[33]	Projection of image features	STARE	81	0.46	92.6
				DRIVE	40	0.32	100
				DIARETDB0	130	0.98	98.5
				DIARETDB1	89	0.98	97.8
				STARE	81		99.75
Lu et al.	2011	[19]	Circular transformation	ARIA	120	5	97.5
				Messidor	1200		98.77
Yu et al.	2012	[15]	Directional matched filter	Messidor	1200	4.7	99
Zubair et al.	2013	[34]	High intensity value of OD	Messidor	1200	-	98.65
Saleh et al.	2014	[35]	Fast fourier transform-based template matching	DRIVE	40	-	100
Yu et al.	2015	[36]	Morphological and vessel convergence approach	DRIVE	40	-	100
				DIARETDB1	89		99.88
				Messidor	1200	-	99.67
Proposed method			Region Matching algorithm	DRIVE	40	100	
				DIARETDB0	130	98.88	
				DIARETDB1	89	98.88	
				DRISHTI	101	100	

Circular transformation is used for segmentation of OD in retinal images. This method yielded accuracy of 99.75%, 97.5%, 98.77% for STARE, ARIA, MESSIDOR databases for detection of OD and 93.4% , 91.7% for STARE, ARIA for segmentation of OD respectively [19]. The localization of OD is done by combining vascular and maximum value of entropy to image area with correct result for 1357 images out of 1361 images [20]. The adaptive morphology is used for detection of OD center and rim with an accuracy of 100% and 97.75%, and SE, SPE of {83.54%, 99.81%}, {92.51%, 99.76%} for DRIVE and DIARETDB1databases respectively [21]. The localization of OC is done by optimal model integration framework, and boundary of OC is detected using multiple super pixel resolution which is integrated and unified. This method yielded an accuracy of 7.12% higher than intra-image learning method [23]. The segmentation and boundary of OC to derive relevant

measurements and depth discontinuity in retinal surface based-approach with error reduction of 16% and 13% for vertical cup to disc diameter relation and CDR calculation are reported [24].

## Conclusions

In the present investigation, an accurate and efficient OD localization using RM, and segmentation of OD and OC using two different algorithms, namely ISPC and AMM are presented. Experiments over four public data sets show localization of OD accuracies of 100%, 98.88%, 98.88% and 100% which is much better than reported results in literature. The average OD and OC segmentation accuracies of 97.23% and 98.42% are obtained for ISPC within which numerous images of structural markers like OD and OC cannot be



segmented by literature reviewed methods and other three methods. In addition, the present technique needs around 7.7 s for both OD detection and OC segmentation, whereas most of the reported results need 13.5 s to perform the same.

The present automated system could be used as DSS towards the detection of glaucomatous development not as a diagnostic

tool. This system complements but does not replace the work of ophthalmologists and optometrists in diagnosis; routine examinations have to be conducted in addition to the fundus image analysis.

**Table 6.** Results for segmentation of OD and OC for the proposed and literature reviewed methods.


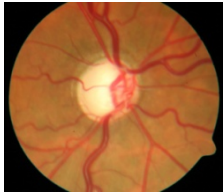
Author	Image Technique	processing	Year	Feature extracted	Database	Number of images	SE (%)	SPE (%)	Overlap error (%)	Success rate (%)	Computation time (s)	Ref
Wong et al.	Variational approach and ellipse fitting	level set and ellipse	2008	CDR	Singapore Malay Eye Study (SiMES)	104			4.81			[37]
Wong et al.	Level set segmentation and Kink based method		2009	CDR	Singapore Eye Research Institute (SERI)	27	81.3	45.5				[38]
Narasimhan et al.	K-Mean clustering and local entropy thresholding		2011	CDR-ISNT ratio	Aravind Eye Hospital (AEH)	36				95		[38]
Ho et al.	Vessel inpainting, circle fitting algorithm and active contour model(ACM)		2011	CDR-ISNT ratio	Chinese Medical University Hospital							[39]
Mishra et al.	Multi-thresholding, ACM		2011	CDR	UK organization Messidor	OD 25, 400						[40]
Yin et al.	Model-based method and Knowledge-based Hough transform		2012	Distance measure	ORIGA	650			9.72 (OD), 32 (OC)			[41]
Narasimhan et al.	k-means and ellipse fitting		2012	CDR-ISNT ratio	AEH	50						[42]
Damon et al.	Vessel Kinking		2012		SERI	67						[43]
Cheng et al.	Super pixel algorithm		2013	CDR	SiMES Singapore Chinese Eye Study (SCES)	650, 1676			9.5, 24.1		10.9 (OD), 2.6 (OC)	[9]
Annu et al.	Wavelet energy features		2013	Energy	Local database	20	100	90		95		[44]
Chandrika et al.	K means pixel clustering & Gabor wavelet transform		2013	CDR Texture								[45]
Ingle et al.	Gradient method		2013									[47]
Cheng et al.	Sparse constraint	dissimilarity	2015	CDR	SiMES, SCES	650, 1676						[48]
Proposed method	ISPC			CDR, ISNT ratio, DOO	DRISHTI	101	97.17, 94.56	95.87, 93.65	2.121.57	97.23, 98.42	6.4, 1.3	

**Table 7.** Results for segmentation of OD and OC for the proposed and literature reviewed methods.

Author	Image Technique	processing	Year	Feature extracted	Database	Number images	of SE (%)	SPE (%)	Overlap error (%)	Success rate (%)	Computation time (s)	Ref
Acharya et al.	SVM, Sequential optimization, NB, forest	minimal random	2011	Texture, Higher order (HOS) spectra features	Kasturba medical college, Manipal	60	-	-	-	91	-	[49]

Acharya et al.	Gabor transformation Principal component analysis	2015	Mean, variance, skewness, Kurtosis, energy, shannon, Renyi, Kapoor entropy	Kasturba medical college, Manipal	510	89.75	96.2	-	93.1	-	[50]
Kolar et al.	Fractal dimension, SVM	2008	-	Own database	30	-	-	-	-	-	[51]
Mookiah et al.	SVM polynomial 1, 2, 3 & RBF	2012	HOS, discrete wavelet transform (DWT)	Kasturba medical college, Manipal	60	93.33	96.67	-	95	-	[52]
Nayak et al.	Mathematical morphology and thresholding, Neural networks	2009	Cup-to-disc ratio, ISNT ratio, distance between OD center to ONH to diameter of OD	Kasturba medical college, Manipal	61	100	80	-	-	-	[10]
Noronha et al.	Linear discriminate analysis, SVM, NB	2014	HOS	Kasturba medical college, Manipal	272	100	92	--	84.72 92.65	-	[53]

**Table 8.** Tuning parameters of neural network classifiers.

Normal/Abnormal	Image	Classification output			
		FFBPNN	DTDNN	RBFEF	RBFFN
Normal		0.9999	1	1	1
Abnormal		0.00085136	0.00004816	0.00001384	0.00001632

## Conflicts of Interest

None

## References

- Lim TC, Chattopadhyay S, Acharya UR. A survey and comparative study on the instruments for glaucoma detection. *Med Eng Phys* 2012; 34: 129-139.
- BREATHER (PENTA 16) Trial Group. Weekends-off efavirenz-based antiretroviral therapy in HIV-infected children, adolescents, and young adults (BREATHER): a randomised, open-label, non-inferiority, phase 2/3 trial. *Lancet HIV* 2016; 3: 421-430.
- Dua S, Acharya UR, Chowriappa P, Sree SV. Wavelet-based energy features for glaucomatous image classification. *IEEE Trans Inf Technol Biomed* 2012; 16: 80-87.
- Kourkoutas D, Karanasiou IS, Tsekouras GJ, Moshos M, Iliakis E, Georgopoulos G. Glaucoma risk assessment using a non-linear multivariable regression method. *Comput Methods Programs Biomed* 2012; 108: 1149-1159.
- Lin JCH, Zhao Y, Chen PJ, Humayun M, Tai YC. Feeling the pressure a parylene based intra ocular pressure sensor. *IEEE Nanotechnology Magazine* 2012; 6: 8-16.
- Xu Y, Xu D, Lin S, Liu J, Cheng J, Cheung CY, Aung T, Wong TY. Sliding window and regression based cup detection in digital fundus images for glaucoma diagnosis. *Med Image Compu Comput Interv* 2011; 14: 1-8.
- Joshi GD, Sivaswamy J, Krishnadas SR. Optic disk and cup segmentation from monocular color retinal images for glaucoma assessment. *IEEE Trans Med Imaging* 2011; 30: 1192-1205.
- Ramakanth S, Babu R. FeatureMatch: a general ANNF estimation technique and its applications. *IEEE Trans Image Process* 2014; 23: 2193-2205.

9. Cheng J, Liu J, Xu Y, Yin F, Wong DW. Superpixel classification based optic disc and optic cup segmentation for glaucoma screening. *IEEE Trans Med Imaging* 2013; 32: 1019-1032.
10. Nayak J, Acharya U R, Bhat PS, Shetty N, Lim TC. Automated diagnosis of glaucoma using digital fundus images. *J Med Syst* 2009; 33: 337-346.
11. Akram MU, Tariq A, Khan SA, Javed MY. Automated detection of exudates and macula for grading of diabetic macular edema. *Computer Methods Programs Biomed* 2014; 114: 141-152.
12. Fuente-Arriaga JA, Felipe-Riverón EM, Garduño-Calderón E. Application of vascular bundle displacement in the optic disc for glaucoma detection using fundus images. *Comput Biol Med* 2014; 47: 27-35.
13. Singh RU, Gujral S. Assessment of disc damage likelihood scale for automated glaucoma diagnosis. *Procedia Computer Science* 2014; 36: 490-497.
14. Hsiao HK, Liu CC, Yu CY, Kuo SW, Yu SS. A novel optic disc detection scheme on retinal images. *Expert Syst Appl* 2012; 39: 10600-10606.
15. Yu H, Barriga ES, Agurto C, Echegaray S, Pattichis MS, Bauman W, Soliz P. Fast localization and segmentation of optic disk in retinal images using directional matched filtering and level sets. *IEEE Trans Technol Biomed* 2012; 16: 644-658.
16. Duanggate C, Uyyanonvara B, Makhanov SS, Barman S, Williamson T. Parameter-free optic disc detection. *Comput Med Imaging Graph* 2011; 35: 51-63.
17. Muramatsu C, Nakagawa T, Sawada A, Hatanaka Y, Hara T, Yamamoto T, Fujita H. Automated segmentation of optic disc region on retinal fundus photographs: Comparison of contour modeling and pixel classification methods. *Comput Methods Programs Biomed* 2011; 101: 23-32.
18. Lu S, Lim JH. Automatic optic disc detection from retinal images by a line operator. *IEEE Trans Biomed Eng* 2011; 58: 88-94.
19. Lu S. Accurate and efficient optic disc detection and segmentation by a circular transformation. *IEEE Trans Med Imaging* 2011; 30: 2126-2133.
20. Mendonca AM, Sousa A, Mendonca L, Campilho A. Automatic localization of the optic disc by combining vascular and intensity information. *Comput Med Imaging Graph* 2013; 37: 409-417.
21. Welfer D, Scharcanski J, Marinho DR. A morphologic two-stage approach for automated optic disk detection in color eye fundus images. *Pattern Recognition Letters* 2013; 34: 476-485.
22. Giachetti A, Ballerini L, Trucco E, Wilson PJ. The use of radial symmetry to localize retinal landmarks. *Comput Med Imaging Graph* 2013; 37: 369-376.
23. Tan NM, Xu Y, Goh WB, Liu J. Robust multi-scale superpixel classification for optic cup localization. *Comput Med Imaging Graph* 2015; 40: 182-193.
24. Joshi GD, Sivaswamy J, Krishnadas SR. Depth discontinuity-based cup segmentation from multiview color retinal images. *IEEE Trans Biomed Eng* 2012; 59: 1523-1531.
25. Sivaswamy J, Krishnadas SR, Datt Joshi G, Jain M, Syed Tabish AU. Drishti-GS: Retinal image dataset for optic nerve head (ONH) segmentation. 2014 IEEE 11th International Symposium Biomedical Imaging (ISBI) Beijing 2015; 53-56.
26. Santhi D, Manimegalai D, Karkuzhali S. Diagnosis of diabetic retinopathy by exudates detection using clustering techniques. *Biomed Eng Appl Basis Commun* 2014; 26: 1450077.
27. Ho CY, Pai TW, Chang HT, Chen HY. An automatic fundus image analysis system for clinical diagnosis of glaucoma. *Proc 5th IEEE Int Conf Complex Intelligent Software Intensive Sys (CISIS 11) IEEE Seoul Republic of Korea* 2011; 559-564.
28. Ibrahim LM. Anomaly network intrusion detection system based on Distributed Time-Delay Neural Network (DTDNN). *J Eng Sci Technol* 2010; 5: 457-471.
29. Youssif AAHAR, Ghalwash AZ, Ghoneim AASAR. Optic disc detection from normalized digital fundus images by means of a vessels direction matched filter. *IEEE Trans Med Imaging* 2008; 27: 11-18.
30. Niemeijer M, Abramoff MD, van Ginneken B. Fast detection of the optic disc and fovea in color fundus photographs. *Med Image Anal* 2009; 13: 859-870.
31. Aquino A, Gegúndez-Arias ME, Marín D. Detecting the optic disc boundary in digital fundus images using morphological, edge detection, and feature extraction techniques. *IEEE Trans Med Imaging* 2010; 29: 1860-1869.
32. Welfer D, Scharcanski J, Kitamura CM, Dal Pizzol MM, Ludwig LW, Marinho DR. Segmentation of the optic disk in color eye fundus images using an adaptive morphological approach. *Comput Biol Med* 2010; 40: 124-137.
33. Mahfouz AE, Fahmy AS. Fast localization of the optic disc using projection of image features. *IEEE Trans Image Process* 2010; 19: 3285-3289.
34. Zubair M, Yamin A, Khan SA. Automated detection of optic disc for the analysis of retina using color fundus image. *Imaging Systems Techniques (IST) 2013 IEEE International Conference Piscataway* 2013: 239-242.
35. Saleh MD, Salih ND, Eswaran C, Abdullah J. Automated segmentation of optic disc in fundus images. 2014 IEEE 10th International Colloquium Signal Processing Piscataway IEEE 2014: 145-150.
36. Yu T, Ma Y, Li W. Automatic localization and segmentation of optic disc in fundus image using morphology and level set. *Medical Information Communication Technology (ISMICT), 2015 9th International Symposium IEEE* 2015: 195-199.
37. Wong DK, Liu J, Lim JH, Jia X, Yin F. Level-set based automatic cup-to-disc ratio determination using retinal fundus images in ARGALI. *Conf Proc IEEE Eng Med Biol Soc* 2008; 2008: 2266-2269.

38. Wong D, Liu J, Lim J, Li H, Wong T. Automated detection of kinks from blood vessels for optic cup segmentation in retinal images. *Medical Imaging Computer-Aided Diagnosis* 2009.
39. Narasimhan K, Vijayarekha K. An efficient automated system for glaucoma detection using fundus image. *J Theor Appl Inform Technol* 2011; 33: 104-110.
40. Mishra M, Nath MK, Dandapat S. Glaucoma detection from color fundus images. *Int J Comp Commun Technol* 2011; 2: 7-10.
41. Yin F, Liu J, Wong DWK, Tan NM, Cheung C, Baskaran M, Aung T, Wong TY. Automated segmentation of optic disc and optic cup in fundus images for glaucoma diagnosis. *Proc 25th IEEE Int Symp Comp Based Med Sys (CBMS 12)* 2012; 1-6.
42. Narasimhan K, Vijayarekha K, Jogi Narayana KA, Siva Prasad P, Satish Kumar V. Glaucoma detection from fundus image using opencv. *Res J Appl Sci Eng Technol* 2012; 4: 5459-5463.
43. Annu N, Justin J. Automated classification of glaucoma images by wavelet energy features. *Int J Eng Technol* 2013; 5: 1716-1721.
44. Chandrika S, Nirmala K. Analysis of CDR detection for glaucoma diagnosis. *Int J Eng Res Appl* 2013; 2: 23-27.
45. Damon WWK, Liu J, Meng TN, Fengshou Y, Yin WT. Automatic detection of the optic cup using vessel kinking in digital retinal fundus images. *Proc 9th IEEE International Biomedical Imaging Nano Macro (ISBI 12)* 2012; 1647-1650.
46. Ingle R, Mishra P. Cup segmentation by gradient method for the assessment of glaucoma from retinal image. *Int J Eng Trends Technol* 2013; 4: 2540-2543.
47. Bock R, Meoer J, Michelson, Nyl LG, Hornegger J. Classifying glaucoma with image-based features from fundus photographs. *Proc 29th DAGM Conf Pattern Recognit* 2010; 355-364.
48. Cheng J, Yin F, Wong DWK, Tao D, Liu J. Sparse dissimilarity-constrained coding for glaucoma screening. *IEEE Trans Biomed Eng* 2015; 62: 1395-1403.
49. Acharya UR, Dua S, Du X, Chua CK. Automated diagnosis of glaucoma using texture and higher order spectra features. *IEEE Trans Inform Technol Biomed* 2011; 15: 449-455.
50. Acharya UR, Ng EY, Eugene LW, Noronha KP, Min LC, Nayak KP, Bhandary SV. Decision support system for the glaucoma using Gabor transformation. *Biomedical Signal Processing and Control* 2015; 15: 18-26.
51. Kolar R, Jan J. Detection of glaucomatous eye via color fundus images using fractal dimensions. *Radioengineering* 2008.
52. Mookiah MR, Acharya UR, Lim CM, Petznick A, Suri JS. Data mining technique for automated diagnosis of glaucoma using higher order spectra and wavelet energy features. *Knowledge-Based Systems* 2012; 33: 73-82.
53. Noronha KP, Acharya UR, Nayak KP, Martis RJ, Bhandary SV. Automated classification of glaucoma stages using higher order cumulant features. *Biomedical Signal Processing and Control* 2014; 10: 174-183.

#### \*Correspondence to

Karkuzhali S

Department of Information Technology

National Engineering College

Tamil Nadu

India